

# PROCEEDINGS OF SPIE

[SPIDigitalLibrary.org/conference-proceedings-of-spie](https://SPIDigitalLibrary.org/conference-proceedings-of-spie)

## Characterization of asymmetric cross-polarization coupling between microresonator whispering-gallery modes

Sandoval, Karleyda, Rosenberger, A.

Karleyda Sandoval, A. T. Rosenberger, "Characterization of asymmetric cross-polarization coupling between microresonator whispering-gallery modes," Proc. SPIE 11700, Optical and Quantum Sensing and Precision Metrology, 117002R (5 March 2021); doi: 10.1117/12.2586663

**SPIE.**

Event: SPIE OPTO, 2021, Online Only

# Characterization of asymmetric cross-polarization coupling between microresonator whispering-gallery modes

Karleyda Sandoval and A. T. Rosenberger\*

Department of Physics, Oklahoma State University, Stillwater, OK, USA 74078-3072

## ABSTRACT

Induced transparency and attenuation are observed in fiber-coupled microresonators due to coupling between coresonant whispering-gallery modes of orthogonal polarizations. Theoretical analysis has shown that this cross-polarization coupling is asymmetric (or nonreciprocal); the coupling from TE to TM generally has a different strength than TM to TE coupling, and the strengths depend on the mode numbers. In an experiment where one polarization is input and the outputs of both polarizations are simultaneously detected by matched detectors, the two coupling strengths are determined by fitting the experimental output spectra to a model. Comparison to theory may then lead to identification of the two modes involved, even when the microresonator dimensions are large compared to the wavelength. Some theoretical results that give similar coupling strengths to those observed in the experiment are presented to give an estimate of typical mode numbers involved.

**Keywords:** microresonator, whispering-gallery modes, induced transparency, nonreciprocal cross-polarization coupling

## 1. INTRODUCTION

Microresonator systems can exhibit coupled-mode induced transparency (CMIT) and Autler-Townes splitting (ATS) with pulse delay, and coupled-mode induced attenuation (CMIA) with pulse advancement, when there is coupling between two coresonant modes.<sup>1-3</sup> These behaviors may be exploited for numerous applications such as signal processing and optical sensing.<sup>4-6</sup> Polarization effects are of growing interest, and the mode coupling under study in this work is cross-polarization coupling, resulting from the spin-orbit interaction of light in a microresonator's whispering-gallery modes (WGMs).<sup>7</sup> The interaction between the spin and extrinsic orbital angular momentum of light in a WGM causes a weak polarization rotation, resulting in cross-polarization coupling (CPC). This is made possible by slight axial asymmetry of the resonator, for example, a hollow bottle resonator (HBR). The different axial extent of the coupled modes, one TE (transverse electric) and one TM (transverse magnetic), then results in their coupling being nonreciprocal. Here we present a method for experimentally determining the CPC strengths of TE to TM coupling and TM to TE coupling.

In previous work, the throughput spectrum of the input polarization has been studied to analyze the CMIT, ATS, and CMIA features and find the CPC strength by fitting to a model.<sup>1</sup> If the CPC amplitudes are  $t_{21}$  for coupling from mode 1 (input) to mode 2 and  $-t_{12}$  for 2 to 1 coupling (see Fig. 1), the destructive interference that gives CMIT comes from light coupled from 1 to 2 and back into 1, so that this contribution to the intracavity mode 1 field amplitude picks up a factor of  $-T_c = -t_{21}t_{12}$ . Model fitting then determines  $T_c$ . In other previous work, the CPC strength  $T_c$  has also been determined by amplitude-modulating the input.<sup>8,9</sup> Finding the modulation frequency that gives the minimum amplitude of the modulated mode 1 throughput on resonance gives a value of  $T_c$  that agrees with the value determined by model fitting, at least in the case of CMIT or ATS. (If  $T_c$  is large enough, there is actual frequency splitting and the IT feature evolves into ATS.<sup>1</sup>)

In the work presented here, in addition to fitting the mode 1 throughput, the mode 2 throughput is also fitted, determining the ratio  $b = t_{21}/t_{12}$ , since the mode 2 throughput amplitude is proportional to  $t_{21}$ . The fact that throughput on mode 2 is observed is evidence for the existence of CPC, and knowing  $b$  and  $T_c$  allows us to determine both  $t_{21}$  and  $t_{12}$ , demonstrating the nonreciprocity of CPC. Also,  $T_c$  and  $b$  are calculated, using the theory presented in Ref. 7, for a few representative sets of mode numbers that give values of  $T_c$  and  $b$  similar to those determined experimentally. These calculations give examples of what the transverse profiles of typical cross-polarization coupled modes might look like.

\*atr@okstate.edu; phone 1 405 744-6742; fax 1 405 744-6811; rosenberger.okstate.edu

## 2. MODEL AND THEORY

### 2.1. Ring cavity model

We use a ring cavity model as shown in Fig. 1. In Fig. 1, the subscripts 1 and 2 refer to the two orthogonal polarizations.  $E_{fj}$  is the input amplitude of polarization  $j$  (only polarization 1 is input, so  $E_{f2} = 0$ ), and

$$E_{rj} = r_j E_{fj} + it_j E_{sj}, \quad (1)$$

is the throughput amplitude of polarization  $j$ .  $E_{sj}$  is the intracavity mode amplitude just before output coupling, and the input/output coupling coefficient is  $it_j$ , with  $r_j^2 = 1 - t_j^2 = 1 - T_j$ . The input and output coupling coefficients are taken to be equal, as described in Ref. 1.

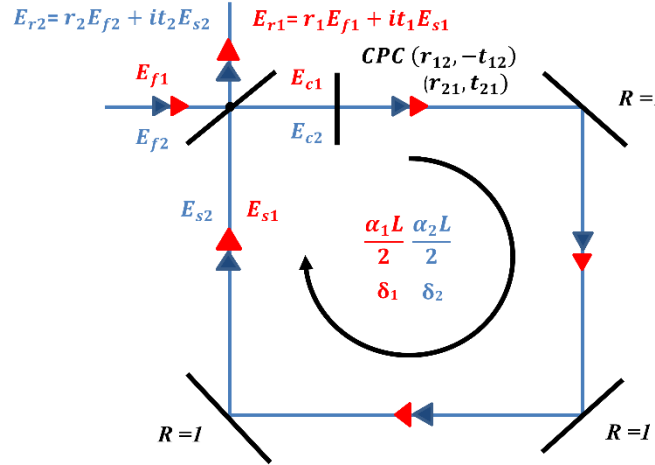


Fig. 1. Ring cavity model representing tapered-fiber coupling to a microresonator with intracavity cross-polarization coupling..

In Fig. 1,  $\delta_j$  and  $\alpha_j L$  are the round-trip phase (modulo  $2\pi$ ) and intrinsic loss for mode  $j$ ;  $L$  is the resonator circumference. Cross-polarization coupling is represented in Fig. 1 as an effective intracavity wave plate and expressed by the coefficients  $t_{12}$  and  $t_{21}$ , where  $t_{12}^2 = 1 - r_{12}^2$  and  $t_{21}^2 = 1 - r_{21}^2$  are the polarization rotation probabilities per round trip, called  $T_s$  and  $T_p$  in Ref. 7.

The intracavity mode amplitudes  $E_{sj}$  satisfy the following time evolution equations:

$$\begin{aligned} \frac{d}{dt} E_{s1} &= -\gamma_1 E_{s1} - \frac{t_{12}}{\tau_{r1}} E_{s2} + \frac{it_1}{\tau_{r1}} E_{f1} \\ \frac{d}{dt} E_{s2} &= -\gamma_2 E_{s2} + \frac{t_{21}}{\tau_{r2}} E_{s1} + \frac{it_1 t_{21}}{\tau_{r2}} E_{f1} \end{aligned}, \quad (2)$$

With these and Eq. (1), the time evolution of the throughput amplitudes can be found. In Eqs. (2),  $\tau_{rj} = n_j L / c$  is the round-trip time for mode  $j$ , where  $n_j$  is the effective refractive index of the mode, and

$$\gamma_j = \frac{T_j + \alpha_j L}{2\tau_{rj}} - i \frac{\delta_j}{\tau_{rj}} = \kappa_j (1 + i\theta_j), \quad (3)$$

with  $\kappa_j$  being the amplitude decay rate, or half the inverse of the photon lifetime in mode  $j$ , and  $\theta_j$  being the offset of the resonant frequency of mode  $j$  from the input frequency in units of half the mode linewidth.

All parameters appearing in Eqs. (1)-(3) with the exception of  $t_{21}$  and  $t_{12}$  are related to experimentally measurable quantities, such as quality factor, resonant dip depth, coupling regime, and input detuning from co-resonance, as described

in Ref. 1. The model is solved in steady state, and  $\left| \frac{E_{r1}}{E_{f1}} \right|^2$  and  $\left| \frac{E_{r2}}{E_{f1}} \right|^2$ , as functions of  $\delta$  (proportional to detuning of input frequency from co-resonance), are plotted and fit to the experimental throughput spectra of modes 1 and 2 respectively, by choosing values of the two fitting parameters  $T_c$  and  $b$ . A good fit thus determines  $T_c$  and  $b$  from experimental data, demonstrating (if  $b \neq 1$ ) the nonreciprocity of CPC.

## 2.2. Theory of CPC

As described in detail in Ref. 7, in order to have CPC from the optical spin-orbit interaction, the resonator must be axially asymmetric. An asymmetry factor is estimated from measurements on typical HBRs fabricated in the lab. This asymmetry means that the average value of the axial component of the propagation constant of the light in the incident WGM will be nonzero. This makes CPC possible, and its strengths (both  $t_{21}^2$  and  $t_{12}^2$ ) can then be calculated by using coupled-mode theory to account for the effects of spatial overlap and phase mismatch between the two orthogonally polarized WGMs.

The radial part of the mode function of a WGM is given in terms of Bessel functions in the three regions of the HBR, interior, silica wall, and exterior. For a small range around a given wavelength (1550 nm), multiple solutions will exist for various combinations of the mode numbers  $m$  (number of wavelengths in the circumference) and  $p$  (number of radial intensity lobes). One solution is found for the TM mode and one for the TE mode, and their radial overlap is calculated. Then for each mode, a value of the mode number  $q$  (number of zeros in an axial intensity plot) is assumed, and the overlap of the two axial profiles, each having the form of a Hermite polynomial of order  $q$  times a Gaussian, is calculated. Then the method of Ref. 7 is used to find the CPC strengths. There are two possibilities; the input mode 1 can be TM or TE, making mode 2 the other polarization. For each possibility, the values of  $T_c$  and  $b$  are calculated.

## 3. EXPERIMENTAL RESULTS

### 3.1. Experimental setup

The experimental setup used is shown in Fig. 2. The tunable diode laser is scanned in frequency and its free-space beam passes through an acousto-optic modulator. Wave plates and a compression-based polarization controller are used to control the input polarization. The coupling fiber is made adiabatically bi-tapered and brought into contact with the HBR in its equatorial plane using a 3D translation stage (not shown). The HBR is mounted on a piezo-controlled holder for strain tuning. The length of fiber after the HBR is kept short and straight to preserve the polarization.

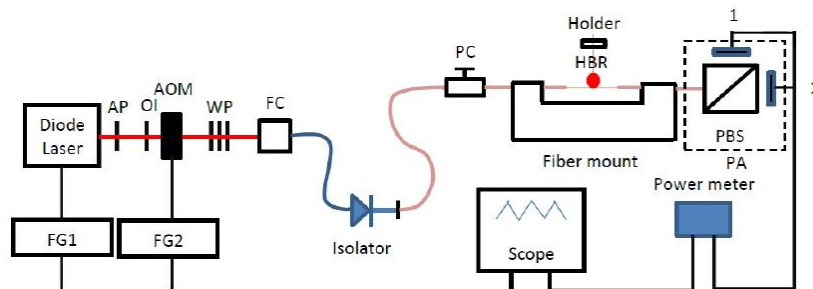


Fig. 2. Experimental setup.

In all cases, the resonator is kept inside an acrylic box to minimize temperature fluctuations and other effects of air movement. The output signal is sent to a polarization analyzer (PA), which includes a polarizing beam splitter (PBS) plus two matched fast detectors and can be rotated about the fiber axis so that either detector can detect either polarization. For data analysis, the detector signals are separately input to the oscilloscope, without using the power meter shown in Fig. 2.

### 3.2. Preliminary results

Light of one polarization is input, and the HBR is strain-tuned to TE-TM coresonance, resulting in the throughput spectrum of the input polarization showing an ATS feature, while the output of the other polarization shows a peak resulting from intracavity CPC. Individual mode parameters are measured by tuning away from coresonance and using input of the two polarizations sequentially. Those parameters are, for mode  $j$ : quality factor  $Q_j$ , relative throughput dip depth  $M_j$ , and the coupling regime. In addition, the mistuning from coresonance  $\Delta$  is estimated. Using those parameters, the model is fitted, using the method described in Ref. 1, to the experimental spectral traces by choosing values of the two free parameters  $T_c$  and  $b$ . Figures 3-5 show three cases. The outer radius of the HBR is given in each case; also, based on the method of HBR fabrication as described in Ref. 10 but without using the hydrofluoric acid etching solution to thin the silica wall, the inner radius is estimated to be  $75.5 \mu\text{m}$  when the outer radius is  $90 \mu\text{m}$ , and  $87.2 \mu\text{m}$  when the outer radius is  $100 \mu\text{m}$ .

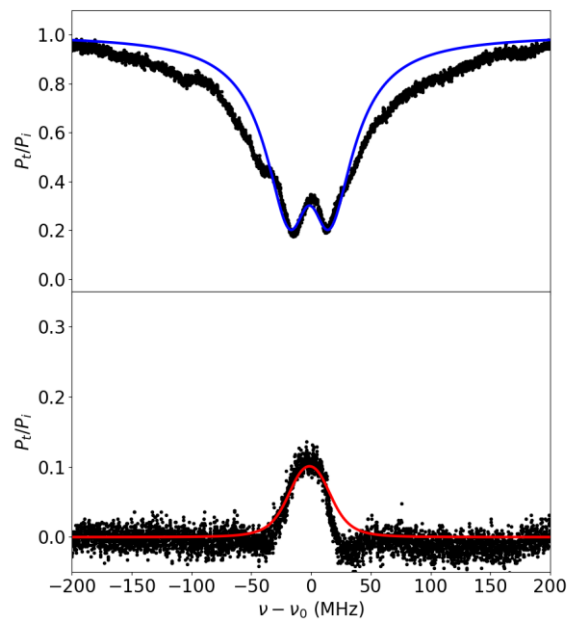


Fig. 3. ATS with 100- $\mu\text{m}$ -radius HBR and TE input. Experimental (black traces) and numerical fitting (blue and red lines) throughput spectra. Parameter values:  $Q_1 = 3.13 \times 10^6$ ,  $Q_2 = 7.29 \times 10^6$ ;  $M_1 = 0.923$  (undercoupled),  $M_2 = 0.296$  (undercoupled);  $\Delta = 0$ . From the fit it is found that  $T_c = 8.91 \times 10^{-8}$  and  $b = 3.7$ .

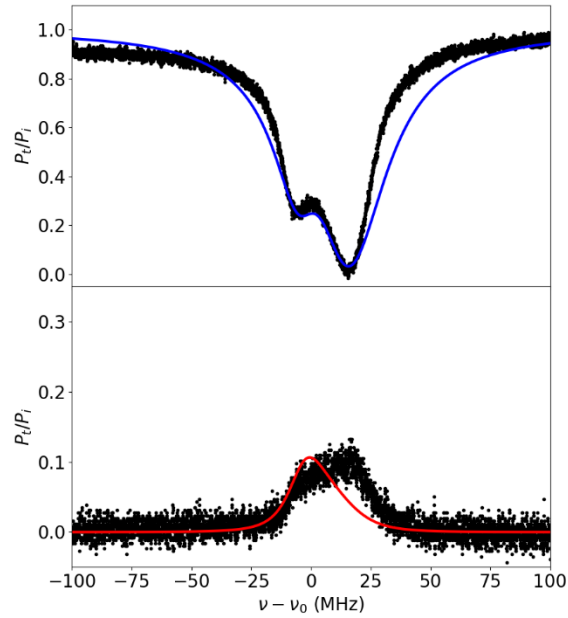


Fig. 4. ATS with 90- $\mu\text{m}$ -radius HBR and TM input. Experimental (black traces) and numerical fitting (blue and red lines) throughput spectra. Parameter values:  $Q_1 = 4.51 \times 10^6$ ,  $Q_2 = 1.186 \times 10^7$ ;  $M_1 = 0.99$  (undercoupled),  $M_2 = 0.11$  (overcoupled);  $\Delta = -11.18$  MHz. From the fit it is found that  $T_c = 6.76 \times 10^{-8}$  and  $b = 0.34$ .

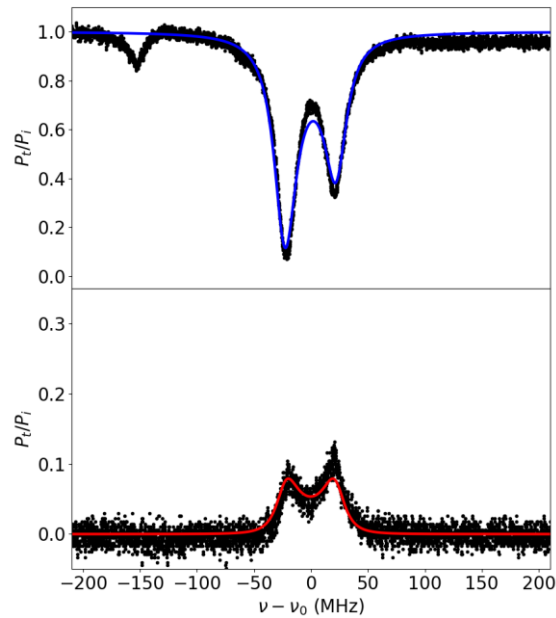


Fig. 5. ATS with 90- $\mu\text{m}$ -radius HBR and TM input. Experimental (black traces) and numerical fitting (blue and red lines) throughput spectra. Parameter values:  $Q_1 = 8.05 \times 10^6$ ,  $Q_2 = 8.05 \times 10^6$ ;  $M_1 = 0.566$  (undercoupled),  $M_2 = 0.566$  (undercoupled);  $\Delta = 13.08$  MHz. From the fit it is found that  $T_c = 1.38 \times 10^{-7}$  and  $b = 1.01$ .

In Figs. 3 and 4, the experimental peak on the orthogonal-polarization output has a shape that is slightly different from the prediction of the model. This is most likely due to interaction with another mode of the same polarization, slightly overlapping in frequency with the mode that couples to the input-polarization mode via CPC. The ratio of coupling

strengths (input→orthogonal to orthogonal→input) is given by  $b^2$ ; for the three cases of Figs. 3-5, the ratio of coupling strengths (TE→TM to TM→TE) thus varies from 13.7 to 8.65 to 0.98.

#### 4. PRELIMINARY THEORETICAL RESULTS

Three cases were calculated, as described in Section 2.2 above, and the results are shown in Figs. 6-8, where the solid red curves are for the TM modes and the dashed black curves are for the TE modes. The outer radius of the HBR is given in each case; the inner radius is estimated to be  $75.5 \mu\text{m}$  when the outer radius is  $90 \mu\text{m}$ , and  $87.2 \mu\text{m}$  when the outer radius is  $100 \mu\text{m}$ .

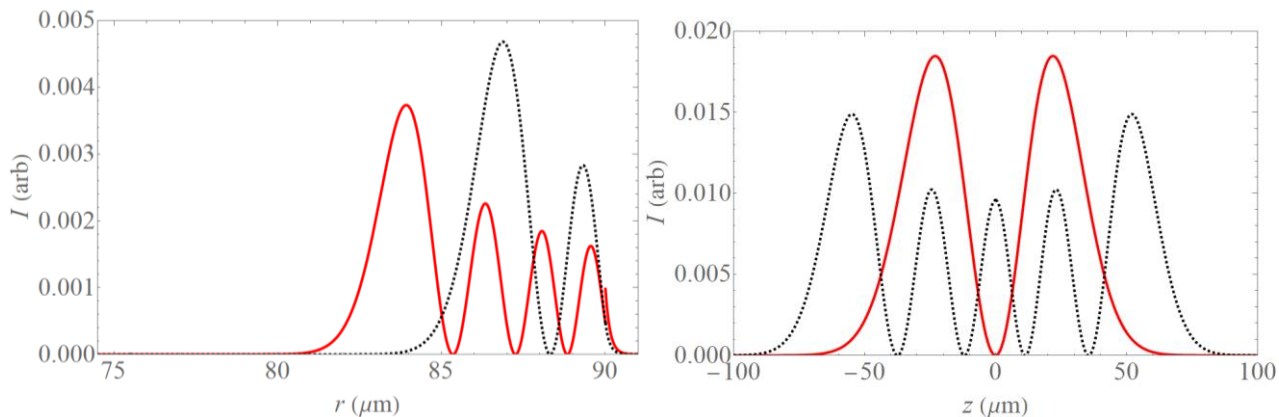


Fig. 6. Radial (left) and axial (right) intensity profiles for a  $90\text{-}\mu\text{m}$ -radius HBR. TM:  $m = 485, p = 4, q = 1$ . TE:  $m = 502, p = 2, q = 4$ . If TE input,  $T_c = 9.93 \times 10^{-8}$  and  $b = 1.66$ ; if TM input,  $T_c = 2.73 \times 10^{-7}$  and  $b = 0.603$ .

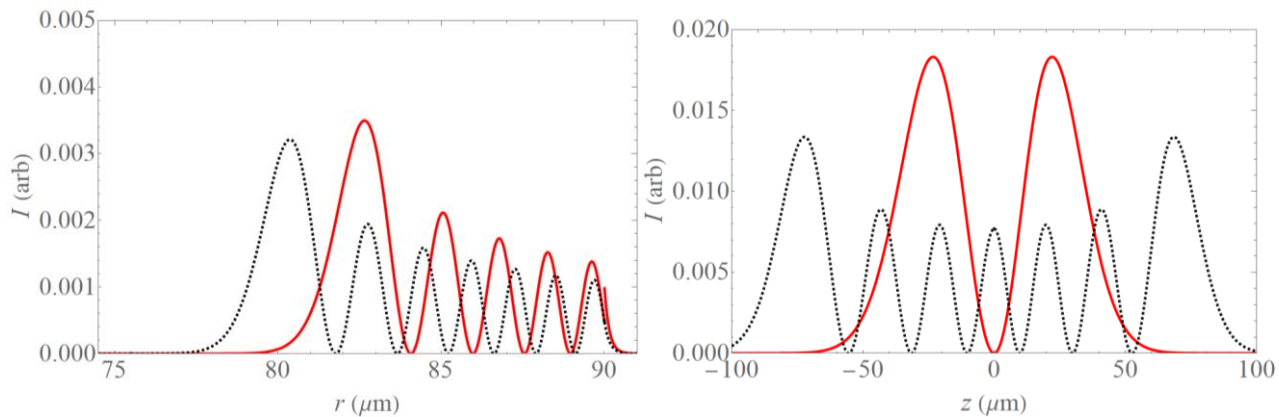


Fig. 7. Radial (left) and axial (right) intensity profiles for a  $90\text{-}\mu\text{m}$ -radius HBR. TM:  $m = 477, p = 5, q = 1$ . TE:  $m = 464, p = 7, q = 6$ . If TE input,  $T_c = 5.59 \times 10^{-8}$  and  $b = 2.06$ ; if TM input,  $T_c = 2.37 \times 10^{-7}$  and  $b = 0.486$ .

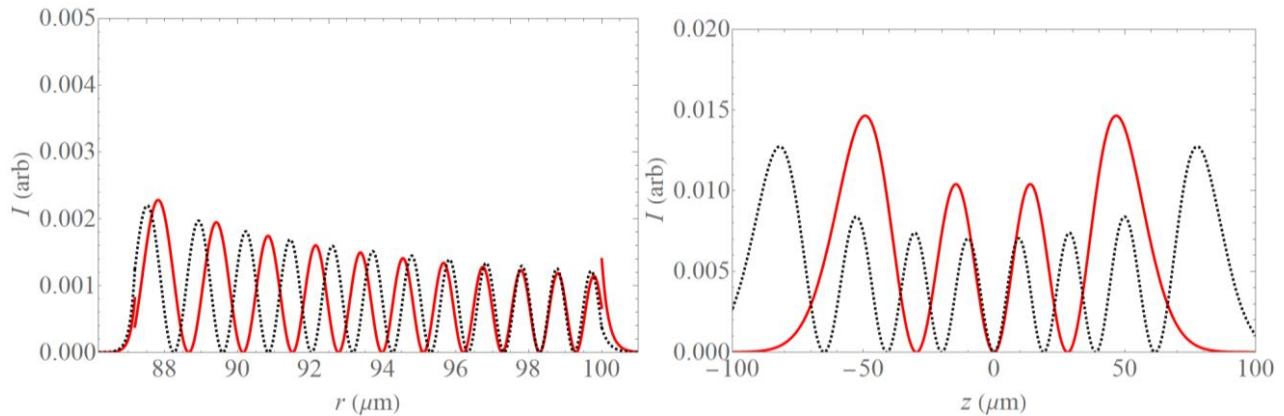


Fig. 8. Radial (left) and axial (right) intensity profiles for a 100- $\mu\text{m}$ -radius HBR. TM:  $m = 489$ ,  $p = 11$ ,  $q = 3$ . TE:  $m = 478$ ,  $p = 12$ ,  $q = 7$ . If TE input,  $T_c = 1.83 \times 10^{-8}$  and  $b = 1.48$ ; if TM input,  $T_c = 3.98 \times 10^{-8}$  and  $b = 0.678$ .

## 5. DISCUSSION

Our earlier theoretical work showed that the cross-polarization coupling that is responsible for CMIT, CMIA, and ATS in a whispering-gallery microresonator is nonreciprocal. Our previous experimental work allowed us to determine the geometrical mean  $T_c$  of the two CPC strengths. Now, by observing the output of the polarization orthogonal to the input polarization, we are able to confirm CPC nonreciprocity and find the two unequal CPC strengths. Further, the theory can be used to find reasonable estimates of the mode numbers of the two WGMs involved.

The fitting method assumes that only two modes are interacting, and it was seen that a third mode near coresonance with the main two can affect the shape of the peak observed in the orthogonal output. The experimental results of Fig. 3, along with the theoretical calculations, are for an empty HBR, so that the internal and external regions both have a refractive index of 1. However, the experiments of Figs. 4 and 5 were done on a water-filled HBR. It was hoped that a mode of high enough radial order could be excited so that the input mode (mode 1) would have a significantly lower  $Q$  than mode 2, owing to absorption losses in the water. This would have produced a greater possibility to see CMIT, not just ATS. This is still under investigation, and it is a relatively simple matter to modify the theory correspondingly.

With the understanding gained here about the orthogonally polarized output 2 under conditions of CPC, its implementation is enabled to a greater degree. Preliminary model results have shown that in some cases the pulse delay of output 2 can be significantly larger than the delay of the output 1 pulse of input polarization. In addition, its amplitude can be greater than that of the output 1 pulse, under certain conditions, if  $b$  is large enough. Thus the non-reciprocity of CPC can have potentially useful consequences.

## ACKNOWLEDGMENTS

We would like to thank Sreekul Raj Rajagopal and Mohamad Junaid Ul Haq for assistance with the experiments.

## REFERENCES

- [1] Bui, K. V., and Rosenberger, A. T., "Coupled-mode-induced transparency and attenuation resulting from cross-polarization coupling," *Phys. Rev. A* 101, 033836 (2020).
- [2] Totsuka, K., Kobayashi, N., and Tomita, M., "Slow light in coupled-resonator induced transparency," *Phys. Rev. Lett.* 98, 213904 (2007).
- [3] Zhou, X., Zhang, L., Pang, W., Zhang, H., Yang, Q., and Zhang, D., "Phase characteristics of an electromagnetically induced transparency analogue in coupled resonant systems," *New J. Phys.* 15, 103033 (2013).



- [4] Foreman, M. R., Swaim, J. D., and Vollmer, F., "Whispering gallery mode sensors," *Adv. Opt. Photon.* 7, 168- 240 (2015).
- [5] Yoshiki, W., Honda, Y., Tetsumoto, T., Furusawa, K., Sekine, N., and Tanabe, T., "All-optical tunable buffering with coupled ultra-high  $Q$  whispering gallery mode microcavities," *Sci. Rep.* 7, 10688 (2017).
- [6] Smith, D. D., Chang, H., Myneni, K., and Rosenberger, A. T., "Fast-light enhancement of an optical cavity by polarization mode coupling," *Phys. Rev. A* 89, 053804 (2014).
- [7] Rosenberger, A. T., Dale, E. B., Bui, K. V., Gonzales, E. K., Ganta, D., Ke, L., and Rajagopal, S. R., "Cross-polarization coupling of whispering-gallery modes due to the spin-orbit interaction of light," *Opt. Lett.*, 44, 4163-4166 (2019).
- [8] Ke, L., Rajagopal, S. R., and Rosenberger, A. T., "Numerical and experimental study of the dynamics of cross-polarization coupling in a whispering-gallery microresonator," *Proc. SPIE* 10904, 109041T (2019).
- [9] Ke, L., Rajagopal, S. R., and Rosenberger, A. T., "Dynamical determination of the strength of cross polarization coupling in a single whispering-gallery microresonator," in preparation.
- [10] Stoian, R.-I., Bui, K. V., and Rosenberger, A. T., "Silica hollow bottle resonators for use as whispering gallery mode based chemical sensors," *J. Opt.* 17, 125011 (2015).